Development and characterization of novel cathode materials for molten carbonate fuel cell

L. Giorgi[a], M. Carewska[a], M. Patriarca[a], S. Scaccia[a], E. Simonetti[a] and A. Di Bartolomeo[b]

[a]*Division of Electrochemical Technologies and Plants,* [b]*Project of Advanced Metallic Materials, ENEA–C.R.E. Casaccia, Via Anguillarese 301, 00060 S. Maria di Galeria (Rome) (Italy)*

Abstract

In the development of molten carbonate fuel cell (MCFC) technology, the corrosion of materials is a serious problem for long-term operation. Indeed, slow dissolution of lithiated-NiO cathode in molten carbonates is the main obstacle for the commercialization of MCFCs. In the search of new, more stable, cathode materials, alternative compounds such as $LiFeO_2$, Li_2MnO_3, and $La_{1-x}Sr_xCoO_3$ are presently under investigation to replace the currently used lithiated-NiO. The aim of the present work was to investigate the possibility to produce electrode based on $LiCoO_2$, a promising cathode material. At first, Li_xCoO_2 powder samples ($0.8 < x < 1.1$) were made by thermal decomposition of carbonate precursors in air. The synthesis processes were monitored by thermal analysis (TGA, DTA). The calcined and sintered powder samples were characterized by X-ray diffraction (XRD) and atomic absorption spectrophotometry (F-AAS). A single phase was detected in all the samples, without any change in crystal structure as a function of lithium content. Porous sintered electrodes were prepared starting from lithium cobaltite powders mixed with different pore-formers by cold pressing and sintering. A bimodal pore-size distribution with a mean pore diameter in the range of 0.15 to 8 μm, a surface area of 2 to 12 m^2/g and a porosity of 10 to 65%, determined by the Hg-intrusion technique, were observed in all the materials. Conductivity measurements were carried out in the temperature range of 500–700 °C, in air. The influence of the deviations from stoichiometry on the electronic properties was determined, the conductivity value of the stoichiometric compound being the lowest. A linear relationship between the electronic conductivity and the sample porosity was found. Solubility testing of the materials was carried out to evaluate their chemical stability in the electrolyte. The sampling method (F-AAS) and square wave voltammetry (SWV) were used to determine the concentration of dissolved cobalt in carbonates melt ($Li_2CO_3/K_2CO_3 = 63/38$ mol%, $pO_2 = 0.33$ atm, $pCO_2 = 0.67$ atm, $T = 650$ °C). The Co content under steady-state conditions, was 6 ppm, i.e., lower than that for Ni from NiO(Li). To test the cathodic performance of the materials, electrochemical impedance spectroscopy (EIS) measurements were carried out to investigate the porous electrode/molten carbonates interface. For this purpose a laboratory-scale MCFC with the same electrolyte as that for the solubility tests was used. The cell was assembled with two identical porous cathodes (fabricated by cold pressing) to avoid any influence from an anode and a reference electrode. With this cell it was possible to determine the influence of atmospheric composition on electrode performance and the long-term stability.

Introduction

Molten carbonate fuel cells (MCFCs) are being extensively investigated in several research and development programs [1–3]. This interest is because the MCFC has

Elsevier Sequoia
SSDI 0378-7753(93)01814-X

promising characteristics for the large-scale electric power generation. These include a potentially high efficiency, the capability of utilizing a wide variety of fossil fuels, the possibility of internal reforming [4], high temperature waste heat for cogeneration, and minimal pollution.

The overall electrochemical half-cell reactions for anodic hydrogen oxidation and cathodic oxygen reduction are as follows:

$$H_2 + CO_3^{2-} \longrightarrow H_2O + CO_2 + 2e^- \quad (1)$$

$$0.5O_2 + CO_2 + 2e^- \longrightarrow CO_3^{2-} \quad (2)$$

and the final product being water:

$$H_2 + 0.5O_2 \longrightarrow H_2O \quad (3)$$

The carbonate ions generated at the cathode and consumed at the anode, are transferred through a porous ceramic matrix (γ-$LiAlO_2$) filled with an alkaline carbonate melt. The mechanisms of both the anodic and cathodic processes are very complex, mainly due to the presence of two bimodal porous gas-diffusion electrodes. As well known, the overall process is usually under mixed control (kinetic, mass transfer and ionic conduction) in this type of electrode.

The state-of-the-art device has the following characteristics:

(i) an operating temperature ranging from 600 to 700 °C;

(ii) a porous nickel anode containing a suitable antisintering additive (usually chromium, or alumina, i.e., aluminium);

(iii) a porous nickel oxide cathode (oxidized and lithiated *in situ*);

(iv) a lithium aluminate matrix ('tile') impregnated with Li/K carbonate electrolyte generally at the eutectic composition (Li/K = 62/38 mol%).

This MCFC configuration is affected by two problems: the corrosion of structural materials and cathode dissolution. The slow dissolution of NiO(Li) in the electrolyte [5–7] may be the main obstacle for the MCFC commercialization. As a result, cathode material is dispersed and transported inside the electrolyte, due to the concentration gradients and electric field in the tile, which contains an oxygen concentration gradient form the cathode to the anode. Therefore, in certain regions between the electrodes, the pO_2 values become lower than those at which the NiO is stable [8]. In these zones, metallic nickel deposition is possible, due to the reduction by hydrogen coming from the anode. So, islands of metallic nickel precipitate inside the tile, giving a nickel ion gradient is present. This gradient allows continuous transport of cathodic material from the electrode/electrolyte interface to the bulk of the electrolyte, giving further deposition of metallic nickel. Eventually the cell fails either by internal short-circuits or depletion of cathodic material.

To solve this problem, new cathodic materials, i.e., alternatives to NiO(Li), must be developed. Such materials must have the following requirements:

(i) high electronic conductivity at 650 °C ($\sigma > 1$ S/cm);

(ii) stability under MCFC operating conditions (650 °C, O_2/CO_2 mixture);

(iii) lower solubility in the cathode environment and higher solubility at the anode than NiO(Li);

(iv) high electrocatalytic activity for the O_2 reduction, and

(v) suitability for the fabrication of porous electrodes with high specific surface area, porosity = 50–80%, and mean pore size = 7–15 μm.

To date, most studies carried out on alternative materials [9–12] have focused on electronic conductivity, and little information is available on the physical-chemical

and electrochemical characteristics related to the fabrication procedures. For these reasons, the results obtained by different authors are often not in agreement.

More than 50 ceramic compounds have been considered as alternative materials: ferrites, cobaltites, manganites, doped metallic oxides, illmenites and spinels. The majority of such materials either are not stable in molten carbonates, or can react with the lithium aluminate. Above all their electrical properties have proved insufficient.

On the basis of the published results, the most promising new materials seem to be lithium-doped metal oxides (Fe, Co, Mn). Lithium ferrite and manganite, may have lower solubility in molten carbonates than NiO, but have unsatisfactory electrical properties. These materials require doping to increase their electrical conductivity, giving problems of choice of the dopant element.

In Japan, the nickel ferrite is under study [8, 13], because of its high stability in molten carbonates. In the USA doped cerium oxide [14] and YAG (yttrium iron garnet) [15] have been investigated. To data, the best performance, relative to that of lithium-doped NiO have been obtained with lithium cobaltite. This material is under investigation by Brown *et al.* (ANL, USA) [16], Plomp *et al.* (ECN, The Netherlands) [17], Bergman *et al.* (Nutek, Sweden) [18], Koch *et al.* (ZSW, Germany) [19].

In the present work, dense, porous Li_xCoO_2 samples were prepared and characterized for physico-chemical and electrochemical properties. The aim was to develop a method of fabricating powders and porous electrodes, to study their structural characteristics, the stability of the materials and the electrochemical properties of stoichiometric and doped lithium cobaltite.

Experimental

Sample preparation and characterization

Samples of $LiCoO_2$ were prepared by thermal decomposition of metal carbonate precursors in air. Lithium and cobalt carbonates (Analar, reagent grade) of desired composition were thoroughly mixed with acetone in a planetary mill for 1 h. The mixtures were transferred in a high purity alumina crucible and slowly heated in the temperature range of 650–900 °C. The temperature of the synthesis reaction was determinated by thermogravimetric analysis (TGA and DTG). The thermoanalytical curves were recorded on a Du Pont 951 thermogravimetric analyser in air. The precursor compounds and their mixtures were heated to 1000 °C/min. The samples obtained were characterized by X-ray diffraction (XRD) using an Ital Structures IS 86 diffractometer with an Cu Kα radiation source. The percentage of the secondary crystalline Co_3O_4 phase in the samples was determined by measuring the relative intensities of the strong peak ($d = 4.699$ A) for $LiCoO_2$ and the peak ($d = 2.438$ A) for Co_3O_4.

The Li/Co molar ratios were determined after dissolution of the samples in (1:1 v/v) HCl by flame atomic absorption (F-AAS), using a Varian Spectra AA-10 spectrometer. The samples were washed in water and filtered to determine the soluble lithium compounds and to obtain a more precise chemical composition.

Sample powders were pressed into round pellets up to 200 MPa, and then were sintered in the temperature range of 750 to 900 °C. The electric properties of dense pellets (density about 90% of theoretical density) were studied by a.c. and d.c. methods using a four-probe technique with gold point contacts for electric resistivity measurements. Conductivities were measured by a AMEL 551 galvanostat and a HP 34578A multimeter as a function of temperature, in the range of 500 to 700 °C, in different atmospheres. The relationship between the electric conductivity and the sample porosity was also studied.

Sintered porous electrodes were prepared starting from lithium–cobalt oxide powders intimately mixed with different pore-formers (graphite and fine carbon black) by cold pressing, followed by sintering in air at temperatures in the range of 800 to 900 °C. The specific surface area and the pore-size distribution were measured by the Hg-intrusion method. A bimodal pore-size distribution with a mean pore diameter ranging between 0.15 and 8 μm, a surface area of 1 to 12 m^2/g and a porosity of 10 to 65% were observed on all the materials.

Solubility test

Solubility of $LiCoO_2$ of stoichiometric composition was measured by the square wave voltammetry (SWV) technique. The apparatus for the solubility test was similar to that used by other authors [20]. The electrolyte (200 g) was a Li_2CO_3/K_2CO_3 (62/38 mol% eutectic (purity > 99.99%), whose composition was verified by chemical analysis. The mixture was slowly heated in an alumina crucible up to the melting point (496 °C) in air and to 650 °C under a CO_2 stream; at the same time the gold electrodes were slowly introduced in the cell. A sample pellet was crushed into 1 mm diameter particles and added to the molten carbonate. A gas mixture (CO_2/O_2 = 67/33 mol%) (SIO Co.) was flowed at 100 ml/min through the cell and the reference electrode. The SWV measurements were carried out using a EG&G 273A potentiostat. To obtain a calibration curve for the SWV current peak, aliquots of melt were withdrawn using an alumina pipette and cooled in a gold plate. The samples were dissolved in HNO_3, transferred to a 50 ml volumetric flask and analysed for the content of Co by F-AAS with background correction for the interference from the high levels of Li and K in the solution. The detection limit was 1 ppm (Co weight/melt weight).

Electrochemical impedance spectroscopy

To test the cathodic performance of the materials under study, electrochemical impedance spectroscopy (EIS) measurements were carried out on the porous electrode/molten carbonates interface. A laboratory scale MCFC constructed, grown recrystallized alumina with the same electrolyte composition as for solubility tests was used. The cell was assembled with two identical cathodes (Fig. 1) instead of the usual configuration (anode and cathode) to allow elimination of the influence of the counter electrode (in this case the anode), and to avoid the use of a reference electrode which is a source of noise [21].

Two identical porous $Li_{1.05}CoO_2$ electrodes (porosity = 50%, medium pore diameter = 8 μm), with a geometric surface area of 2.6 cm^2 were used. The tile was fabricated by impregnating a porous sintered γ-$LiAlO_2$ disc with a carbonate melt, pre-mixed to the eutectic composition (Li/K = 62/38 mol%). The current collectors were AISI 316 stainless-steel perforated plates.

The cell was heated to the operating temperature (650 ± 2 °C) a 30 °C/h ramp rate, and fed with a cathode gas mixture ($O_2/CO_2/N_2$ = 14/30/56). If not otherwise stated, measurements were carried out at this constant gas composition, at a constant flow rate of 200 ml/min on both electrodes.

The EIS data were determined with a Solartron 1286 and a Solartron 1250 frequency response analyser both controlled by a Hewlett Packard 310 computer. The cell was galvanostatically polarized at zero imposed current with a superimposed 236 $\mu A/cm^2$ sinusoidal signal in the frequency range of 0.1 Hz to 65 kHz. The EIS data files were converted from HP BASIC to DOS format by means of an appropriate software [22] running on a HP Vectra ES/12 computer, upgraded with an HP 83200B

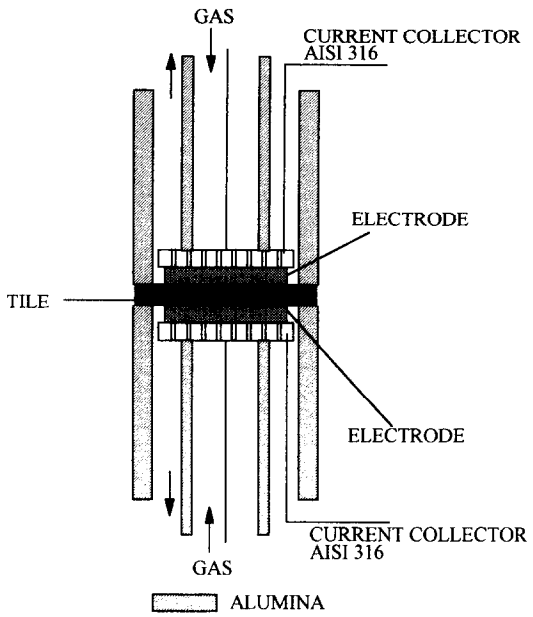

Fig. 1. Schematic view of the alumina molten carbonate fuel cell used for the electrochemical impedance spectroscopy measurements.

language processor card. This operation used NLLS (non-linear least-squares) software [23].

Results and discussion

Synthesis of Li_xCoO_2 compounds

The TG and DTG curves of lithium–cobalt carbonate mixture with Li/Co = 1 are presented in Fig. 2. The TG curve showed a gradual weight loss over the temperature range from 50 to 700 °C, which was followed by a plateau up to 1000 °C.

The DTG maxima of the precursor chemicals were compared with those of their mixture given in Table 1. The maxima at 145 and 267 °C corresponding to dehydration and decomposition of $CoCO_3$ to Co_3O_4, respectively [25], were similar for the precursors and their mixture. The DTG curve of the lithium–cobalt carbonate mixture showed an additional peak, at around 406 °C, whereas the DTG peak between 900 and 950 °C for the transformation of Co_3O_4 to CoO was absent.

The mixture was calcined at 650 °C for 10 h in air, after which XRD patterns of the product indicated formation of $LiCoO_2$ with 0.6 wt.% of Li_2CO_3. No trace of a secondary CoO phase was detected. Chemical analysis gave a composition corresponding to 7.06% Li and 60.10% Co. We conclude that $LiCoO_2$ synthesis reaction takes place in the 300–650 °C temperature range.

A series of Li_xCoO_2 samples ($0.80 \leqslant x \leqslant 1.10$) were prepared by calcination of the starting precursors at 650 °C. XRD patterns indicated the formation of well crystallized phases in all samples. For the $x > 1.00$ compositions extra peaks which may be assigned to Li_2CO_3 and CoO appeared. On prolonged heating at higher temperatures

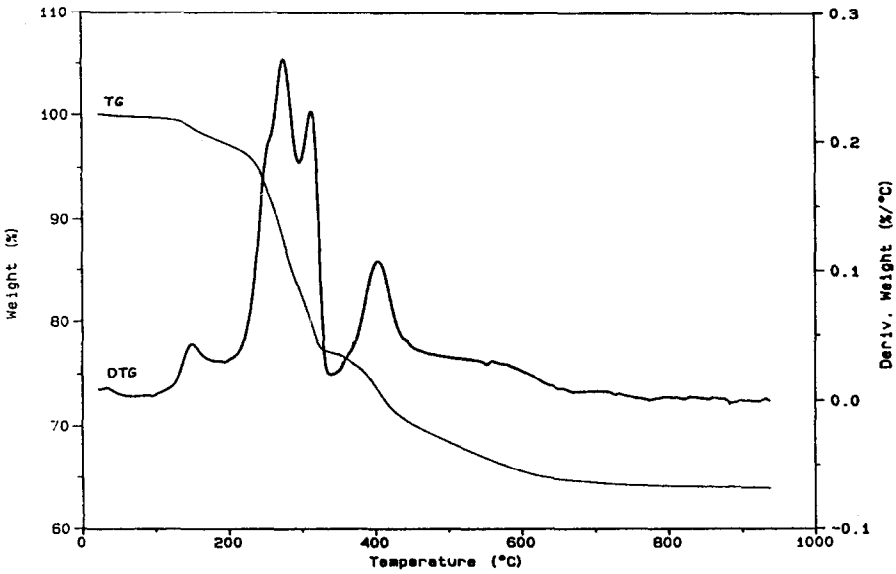

Fig. 2. Thermogravimetric (TG) and derivative thermogravimetric (DTG) curves of $CoCO_3 \cdot xH_2O + Li_2CO_3$ mixture in air.

TABLE 1

DTG maxima of the thermal decompositions of pure precursors and their mixtures

Precursors	Temperature (°C)		Remarks
	Present work	Literature	
Li_2CO_3		723 [24]	Melting point
$CoCO_3 \cdot xH_2O$	128	145 [25]	Loss of water
	269	222 [25]	Two overlapping broad peaks due to $CoCO_3 \rightarrow Co_3O_4$
	306	267	
	908	910 [25]	$Co_3O_4 \rightarrow CoO$
Li_2CO_3	151		
+	277		
$CoCO_3 \cdot xH_2O$	317		
	406		

(800–900 °C), the Li_2CO_3 peak intensity decreased and no secondary CoO phase was detected. These results agreed well with chemical analyses. However, an appreciable amount of unreacted Li_2CO_3 and CoO were seen for the compositions with $x = 0.94$ and $x = 0.80$, even though the synthesis temperature was as high as 900 °C. Table 2 lists the results of chemical analysis of the samples. The results showed that it was not easy to prepare Li_xCoO_2 with $x < 1$. The difficulty in synthesizing these compositions has been reported for the chemical deintercalation of $LiCoO_2$ used as battery cathodes [26].

TABLE 2

Chemical composition of Li_xCoO_2 compounds

Li/Co	Formula
0.80	$Li_{0.86}Co_{1.07}O_2$
0.94	$Li_{0.94}Co_{1.00}O_2$
1.00	$Li_{1.02}Co_{1.02}O_2$
1.01	$Li_{1.02}Co_{1.01}O_2$
1.05	$Li_{1.05}Co_{1.00}O_2$
1.08	$Li_{1.05}Co_{0.97}O_2$
1.10	$Li_{1.06}Co_{0.96}O_2$

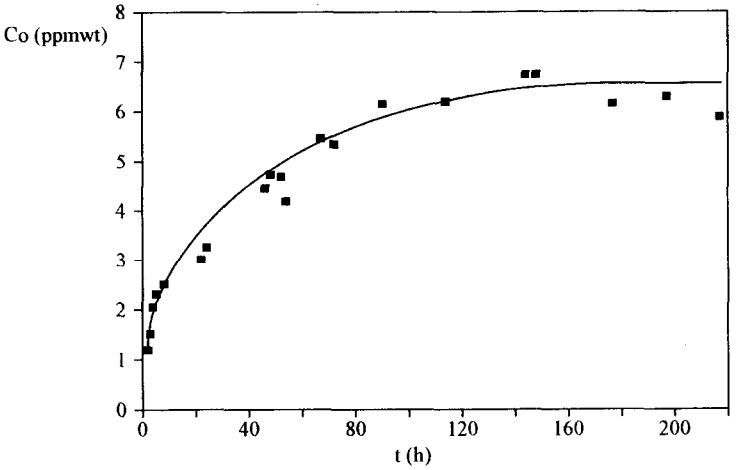

Fig. 3. Dissolution curve of $LiCoO_2$ in molten carbonates (Li/K = 62/38 mol%) at 650 °C and O_2/CO_2 = 33/67 mol%.

Solubility data

The dissolution curve of $LiCoO_2$ in melt carbonate, obtained from SWV data, is depicted in Fig. 3. The Co content increased rapidly with time and the equilibrium solubility (6 ppm_{wt}) was achieved when the Co concentration did not vary by more than $\pm 5\%$ over a three-day period.

Of the few available data on $LiCoO_2$ solubility, those of Veldhuis *et al.* [27] also employed the SWV technique for monitoring the dissolved Co in the molten carbonates. Their results are very similar to our data.

After the solubility test, the $LiCoO_2$ particles were saved by washing the carbonates with 70/30% (v/v) acetic acid/anhydride mixture and analysed by XRD. The XRD patterns indicated that there was no structural changes in the sample.

Electric properties

After preliminary tests, the electric conductivity (C) of Li_xCoO_2 samples was measured by a d.c. technique following the Van der Pauw method [28]. Plots of ln C versus $1/T$ for all investigated lithium compositions are shown in Fig. 4. The curves follow the exponential Arrhenius relationship $C = C^0 \exp(-E_a/kT)$, which is

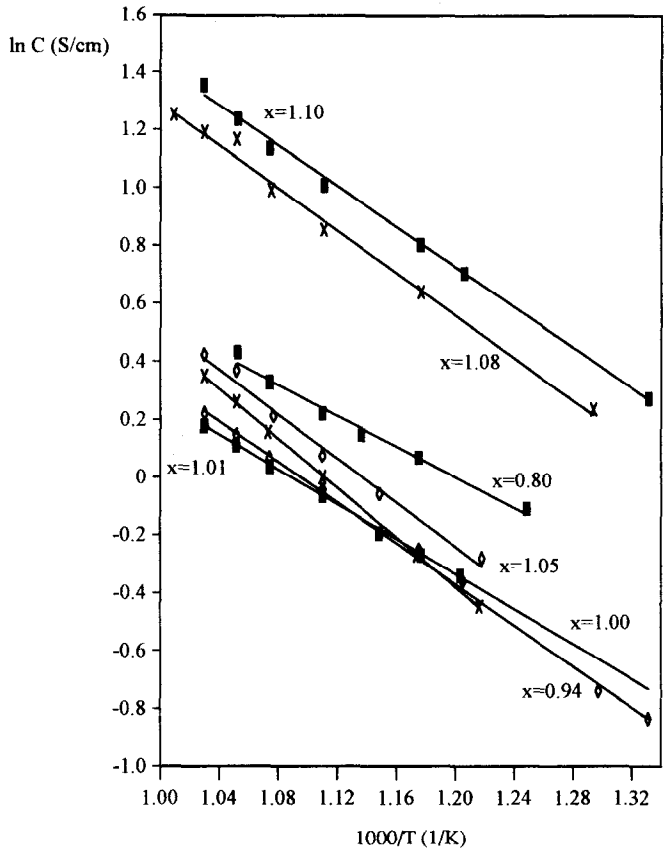

Fig. 4. Arrhenius plot for the electrical conductivity in air of lithium cobaltite with different lithium contents (x).

valid for semiconductors. The values of activation energy extracted from the slope of the curves were a function of the lithium content (Fig. 5). They agree with the published data [29].

Figure 6 shows the variation of the calculated electronic conductivity as a function of x in Li_xCoO_2 at different temperatures. The electric properties of Li_xCoO_2 materials depend on the lithium content, and the electronic conductivity has a minimum value close to the stoichiometric composition. With lithium disintercalation, conductivity increases somewhat, while intercalation increases conductivity significantly. This shows that lithium induces strong p-type semiconductor properties in the compound, and vacancies exist in the cation sublattice that are electrically compensated by positive holes. This results in the formation of higher valent cobalt ions. The electric conductivity is proportional to the concentration of positive holes in the lattice.

As in the case of NiO [30], introduction of lithium into the solid cobaltite forms a solid $Li_2O + Li_xCoO_2$ solution according to the reaction:

$$Li_2O + 0.5O_2 \longleftrightarrow 2Li'_{Co} + 2O_O + 2h' \qquad (4)$$

where Li'_{Co} denotes a lithium ion which has replaced a cobalt ion in the cobalt sublattice

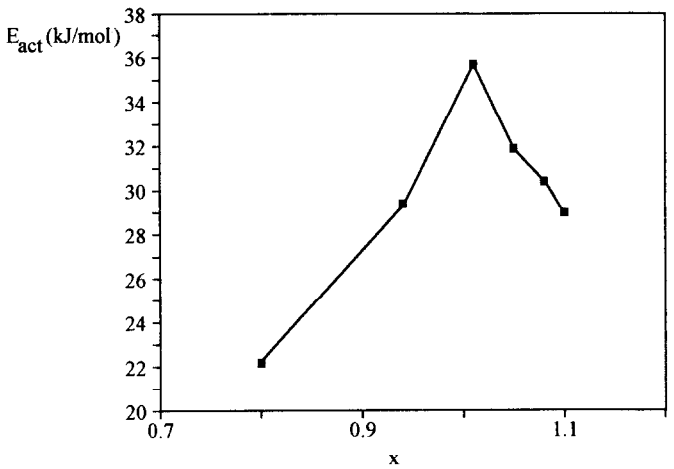

Fig. 5. Dependence of activation energy for the electrical conductivity in air on the lithium content in Li_xCoO_2.

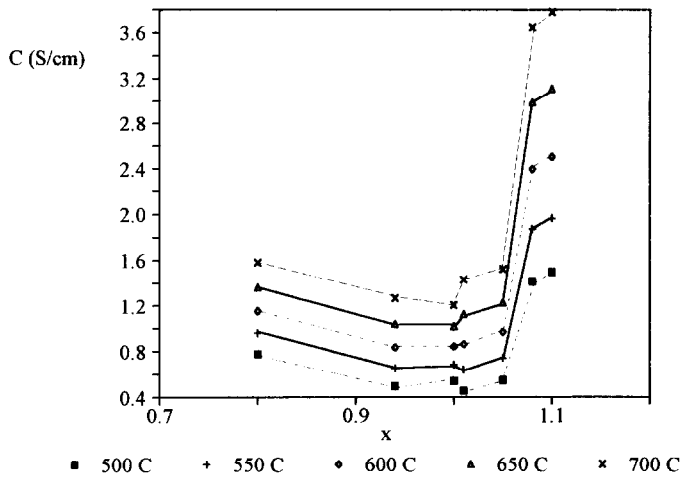

Fig. 6. Influence of lithium content (x) in Li_xCoO_2 on electrical conductivity at different temperatures.

and O_O is an excess oxygen ion on a regular oxygen site. Positive holes h', formed according to the reaction (4), are represented by high-valent Co ions in the lattice. When the lithium concentration exceeds the solubility of Li_2O in Li_xCoO_2, the formation of a higher lithium content oxide can begin:

$$2LiCoO_2 + xLi_2O + x/2O_2 \longleftrightarrow 2Li_{1+x}Co(III)_{1-x}Co(IV)_xO_{2+x} \quad (5)$$

In Li/K carbonate eutectic, where peroxide ions can be postulated to be stable [21, 31], the reactions (4) and (5) can be rewritten in the form:

$$2Li^+ + O_2^{2-} \longleftrightarrow Li'_{Co} + 2O_O + 2h' \quad (3)$$

$$2LiCoO_2 + 2xLi^+ + xO_2^{2-} \longleftrightarrow 2Li_{1+x}Co(III)_{1-x}Co(IV)_xO_{2+x} \quad (4)$$

The electric properties at various atmospheric compositions (air, O_2 CO_2 and O_2/CO_2 mixtures) at 678 °C were investigated for samples with $x=1.05$. To study the influence of pure CO_2 atmosphere on the electrical conductivity, it was necessary to wait for 144 h to obtain stable measurements. A drastic change of electronic conductivity was observed in the absence of oxygen with CO_2 present (Table 3). Presumably selective adsorption of CO_2 on active sites used for hopping of the charge carriers occurs, blocking the conduction mechanism. The fact that the presence of a low-oxygen concentration strongly increases the conductivity induces to think that a competition between O_2 and CO_2 is present and the oxygen adsorption is the fastest process.

The strongly decreasing electrical conductivity in pure CO_2 is in agreement with the relationship between the hole concentration and the partial pressure of O_2 and CO_2 [32], i.e.:

$$[h'] = kpO_2{}^{a} pCO_2{}^{-b} \tag{5}$$

which influences the electric conductivity:

$$C_{h'} = \exp(\mu_{h'}[h']) \tag{6}$$

The activation energy for electric conductivity in the pure CO_2 atmosphere was determined, and its value (37 kJ/mol) was higher than that in air (32 kJ/mol).

A correlation between the fractional porosity (P) on the electrodes and the conductivity was found to follow the expression:

$$\log C = a + n \log(1-P) \tag{5}$$

From the previous relationship, the slope ($n=1.66$) falls inside the literature values ($n=1.5$–2) [33, 34]; therefore it is possible to compare samples having different porosity to calculate the IR loss operating in cells.

EIS spectra analysis

A typical EIS spectrum of $Li_{1.05}CoO_2$ at 650 °C with a corresponding spectrum for NiO(Li) as reference are shown in Fig. 7. Both spectra are depressed at low frequencies due to the effects of porous electrode structure, that for the lithium cobaltite electrode being more evident.

The depression angle (DA) changes its value during operation time (Fig. 8). At first, the DA values are very close to those for NiO(Li) [35], which means the physical structures of the two materials are very similar. However, a fast decrease of DA after about 170 h is observed. Probably this represents a change in the structure of the electrodes due to sintering.

A confirmation of sintering was obtained by pore-size distribution measurements. These were determined for $Li_{1.05}CoO_2$, after which a heat treatment at 900 °C for

TABLE 3

Electric conductivity at 678 °C of $Li_{1.05}CoO_2$ as a function of atmosphere composition

Gas composition		Electric conductivity (S/cm)
O_2 (%)	CO_2 (%)	
0	100	0.22
20	0	1.54
33	67	1.55
100	0	1.56

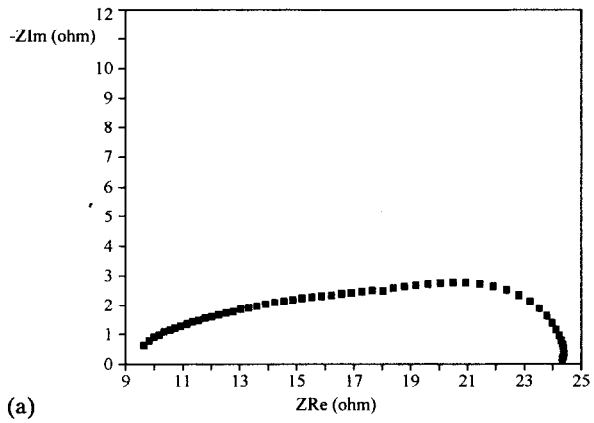

(a)

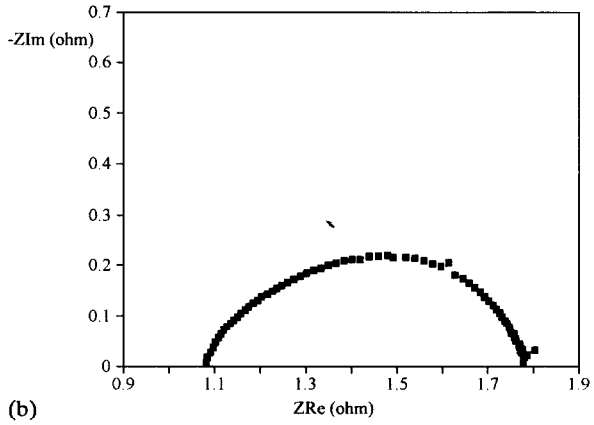

(b)

Fig. 7. EIS spectra of (a) porous $Li_{1.05}CoO_2$ and (b) NiO(Li) electrodes recorded in molten alkaline carbonates (Li/K = 62/38 mol%) at 650 °C ($pO_2 = 0.14$ atm, $pCO_2 = 0.30$ atm, and $pN = 0.56$ atm).

120 h was conducted, and the pore-size distribution was again measured. From the results the heat treatment produces a micro-porosity at $r_p < 0.1$ μm. As a consequence, the total porosity and the specific surface area increase, while the medium pore radius decreases (Table 4).

From the EIS spectra, the electrolytic (R_e) and total polarization (R_p) resistances can be obtained. R_e is the intersection of the high frequency data with the real axis, but in reality its value is the sum of two terms, the resistances of the tile (R_{til}) and the electrode (R_{el}). The value of R_{tile} is time invariant, because the carbonates loss by evaporation can be neglected in the tile used in the present work [36]. Values of R_e and consequently R_{el} decrease with time (Fig. 9), indicating that the conductivity of the lithium cobaltite increases. This phenomenon can be ascribed to the introduction of Li^+ ions into the lithium–cobalt oxide lattice, with the generation of higher valent cobalt ions and the corresponding increase in the hole concentration. The conductivity doubles during this first stage (Fig. 6), along with an increase in lithium content in the cobaltite, with x increasing from $x = 1.05$ to $x = 1.08$.

The value of R_p has a different behaviour with the time. Earlier, its value is low, after 200 h it sharply increases, and after 800 h it finally stabilizes at a constant level.

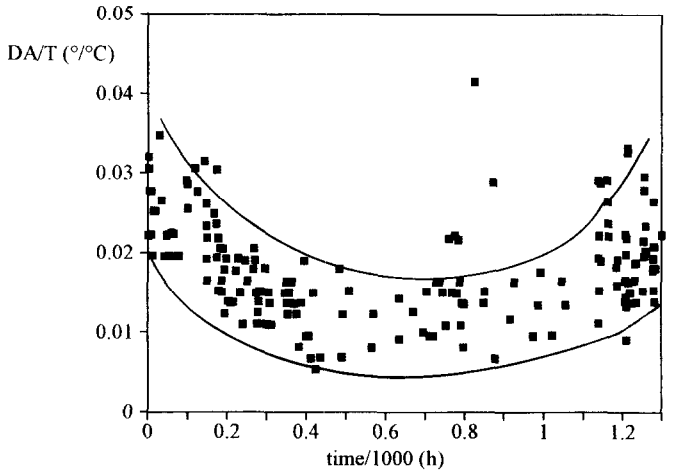

Fig. 8. Time change vs. depression angle in EIS spectra.

TABLE 4

Structural modifications of $Li_{1.05}CoO_2$ after a heat treatment at 900 °C for 120 h

Sample	Porosity (%)	Medium pore radius (μm)	Specific surface area (m^2/g)
As produced	50	3.4	3.9
After heat treatment	41	4.7	1.3

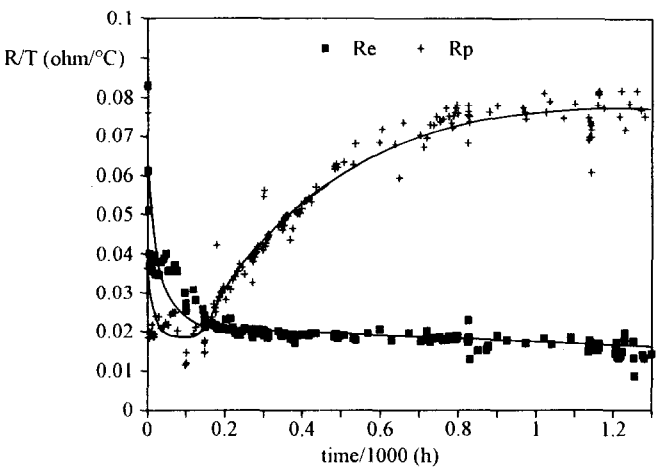

Fig. 9. Time change of electrolyte + electrodes resistance (R_e) and total polarization resistance (R_p), from EIS data.

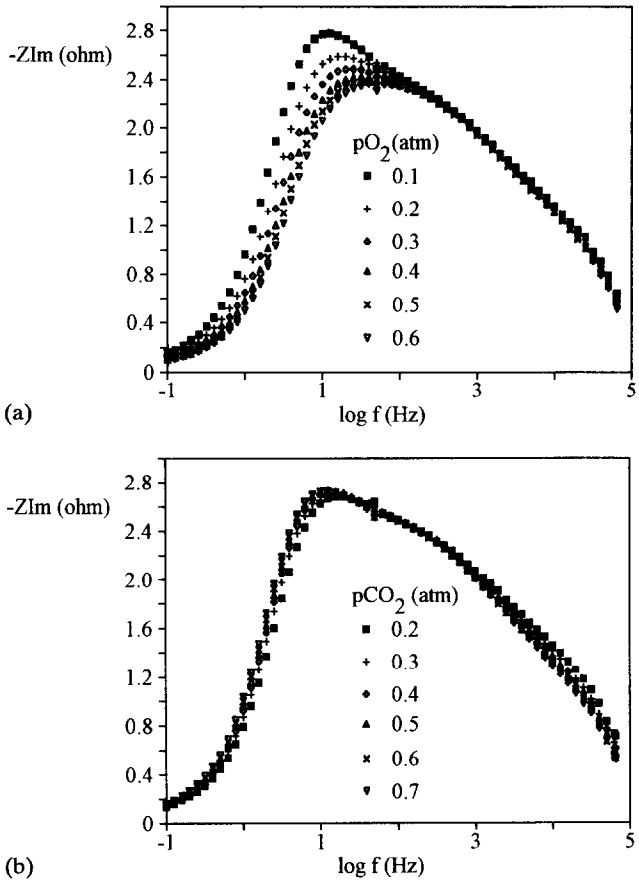

Fig. 10. Influence of the oxygen and carbon dioxide concentration on the imaginary impedance component for $Li_{1.05}CoO_2$.

A comparison between *DA* and R_p shows that the strong increase in polarization resistance coincides with the decrease of the depression angle, while the stabilization of R_p corresponds to a new increase in the *DA*. Further experimental work and data analyses are required to explain this phenomenon.

To determine the influence of the cathodic gas composition on electrode performance, the atmosphere was changed while maintaining constant either the partial pressure of CO_2 or that of O_2. The value of pCO_2 was maintained at 0.30 atm and pO_2 was changed in the range of 0.10 to 0.60 atm, then the pO_2 was maintained at 0.14 atm and pCO_2 changed between 0.20 and 0.70 atm. In this way, it was possible to study the kinetic effect of each gas. An increase in either pO_2 or pCO_2 reduces the total polarization resistance, but changes in pO_2 have the greatest influence. Oxygen affects the charge-transfer resistance because the EIS spectra shape is deformed up to 300 Hz. In contrast, CO_2 has the greatest effect up to 10 Hz, so that mass transport is under CO_2 control, as suggested by Uchida [37] for NiO electrodes. These influences are clearer if the EIS data are plotted as imaginary impedance components as a function of frequency. It is then possible to more effectively compare the behaviour

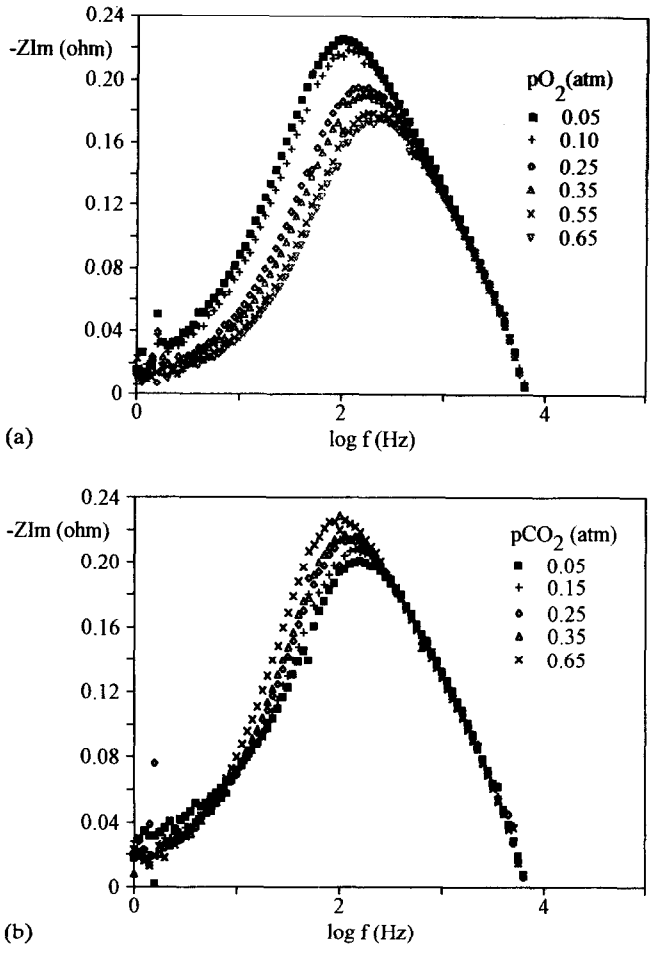

Fig. 11. Influence of the oxygen and carbon dioxide concentration on the imaginary impedance component for NiO(Li).

of lithium cobaltite (Fig. 10) and lithium-doped nickel oxide (Fig. 11). For Li–NiO electrodes the influence of O_2 on the kinetic and diffusion processes is positive, while that for CO_2 is negative; these results agree with the proposed mechanism [38–40] for oxygen reduction in molten carbonates. In the case of lithium cobaltite O_2 has the same influence on kinetics, but CO_2 has a little influence. This indicates that the diffusion process is no longer controlled by CO_2.

The EIS data as a function of gas composition give linear log-log relations between both R_e, and R_p and the partial pressure of O_2 and CO_2 (Fig. 12). Increase in partial pressure reduces the electrode resistance with both O_2 and CO_2, but the effect of oxygen is the more marked. The total polarization resistance is also reduced by increasing pO_2, but it is not affected by an increase of pCO_2, so that O_2 has a controlling influence on electrode kinetics, while CO_2 has a negative effect.

Unlike the NiO cathode [31], the total electric resistivity R_e (electrodes + electrolyte) is strongly influenced by pure CO_2, which gives a value 2.5 times higher then in

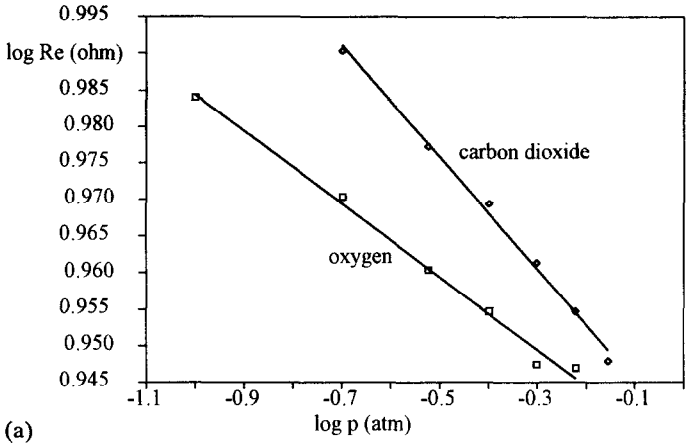

(a)

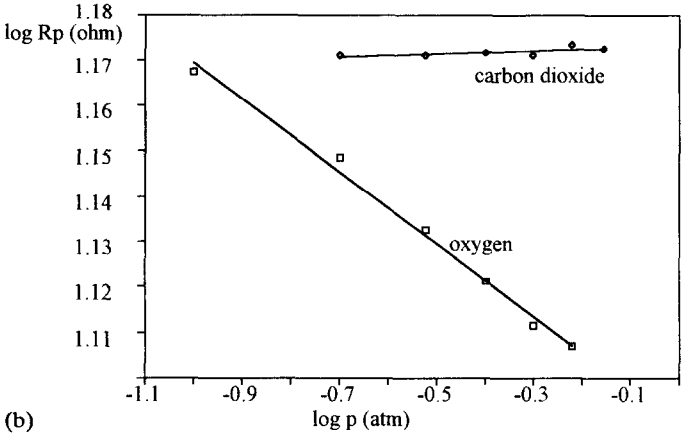

(b)

Fig. 12. The oxygen and carbon dioxide dependence of R_e and R_p.

$O_2/CO_2 = 14\%/30\%$. This result agrees with the electric conductivity measurements of the electrodes outside the cell, c.f., eqns. (8) and (9).

The total electric conductivity of the cell was measured as a function of temperature and the corresponding Arrhenius plot shows good linearity ($r^2 = 0.98$), with an activation energy of 63 kJ/mol. This value is 2.7 times higher than that measured in the same cell for NiO(Li) [41]. This may be explained by the lower conductivity of $LiCoO_2$ (1.2 S/cm) compared with that of NiO(Li) (15 S/cm) [25].

Conclusions

The results of the work can be summarized as follows:

1. The experimental preparation conditions to obtain a series of samples of Li_xCoO_2 powders, with x ranging from 0.80 up to 1.10, starting from carbonates precursors were determined.

2. The powders were characterized by XRD, TG, DTG and F-AAS.

3. The solubility of $LiCoO_2$ was measured (6 ppm), which is lower than that of NiO.

4. The electrical conductivity, under different atmospheres, was determined. Results depended on lithium content, especially for samples with excess of Li. A strong decrease in conductivity was found in pure CO_2 atmosphere.

5. The electrochemical behaviour of a $Li_{1.05}CoO_2$ cathode was studied by mean of EIS in a symmetrical cell. From the depression angle values in the EIS spectra, we conclude that the structure of the electrode is very similar to that of NiO(Li), but it changes with time. That this is probably due to a sintering process as confirmed by pore-size distribution measurements.

6. The electrode resistance decreased during the test period, due to Li^+ intercalation in the lithium–cobalt oxide lattice.

7. Experiments on the influence of gas composition on the total polarization resistance showed a high positive effect of pO_2, which is related to kinetic phenomena. In contrast, pCO_2 had a smaller negative effect on mass transport than is the case with NiO(Li) cathodes.

Acknowledgements

The authors would like to acknowledge E. Giacometti, F. Pallini and R. Tulli for the technical support in the experimental work.

References

1 H. Maru, M. Farooque, I. Paetsch, C. Yuh, P. Patel, J. Doyon and R. Bernard, *Proc. 1992 Fuel Cell Seminar, Nov. 29–Dec. 2, 1992, Tucson AZ, USA*, p. 29.
2 R. Ottervanger, R. Boersma and L. de Vaal, *Proc. 1992 Fuel Cell Seminar, Nov. 29–Dec. 2, 1992, Tucson, AZ, USA*, p. 31.
3 C. Hiari, M. Matsumura, Y. Gonjo, A. Sasaki and E. Nishiyama, *Proc. 1992 Fuel Cell Seminar, Nov. 29–Dec. 2, 1992, Tucson, AZ, USA*, p. 61.
4 D.A. Shores, J.R. Selman, S. Isran and E.T. Ong, *Proc. Molten Carbonate Fuel Cell Technology*, Vol. 90-16, The Electrochemical Society, Pennington, NJ, USA, 1990.
5 M.L. Orfield and D.A. Shores, *J. Electrochem. Soc., 136* (1989) 2862.
6 J.D. Doyon, T. Gilbert and G. Davies, *J. Electrochem. Soc., 134* (1987) 3035.
7 C.E. Baumgartner, *J. Am. Ceram. Soc., 67* (1984) 460.
8 K. Ota, S. Mitsushima, K. Kato and N. Kamiya, *Proc. Molten Carbonate Fuel Cell Technology*, Vol. 90-16, The Electrochemical Society, Pennington, NJ, USA, 1990.
9 J.L. Smith, G.H. Kucera and A.P. Brown, *Proc. Symp. Fuel Cells, Oct. 14–19, 1990, Seattle, WA, USA*, p. 226.
10 J.L. Smith, G.H. Kucera and A.P. Brown, Lithium manganite development as a molten carbonate fuel cell cathode, *EPRI Rep. GS-7288*, May 1991.
11 C.E. Baumgartner, R.H. Arendt, C.D. Jacovangelo and B.R. Karas, *J. Electrochem. Soc., 131* (1984) 2217.
12 M. Franke and J. Winnick, *J. Appl. Electrochem., 19* (1989) 1.
13 K. Ota, S. Mitsushima and N. Kamiya, *Denki Kagaku, 56* (1988) 435.
14 M. De Gurie, M.J. Shingler and E. Dincer, Doped cerium oxide for molten carbonate fuel cell cathodes, *EPRI Rep. ER-6983*, Sept. 1990.
15 A. Khandar, Yttrium iron garnet as a molten carbonate fuel cell cathode, *EPRI Rep. TR-101 069*, Sept. 1992.
16 A.P. Brown, G.H. Kucera, M.F. Roche, D.D. Chu and E. Indachochea, *Proc. 1992 Fuel Cell Seminar, Nov. 29–Dec. 2, 1992, Tucson, AZ, USA*, p. 125.

17 L. Plomp, J.B.J. Veldhuis, E.F. Sitters and S.B. van der Molen, *J. Power Sources, 39* (1992) 369–373.
18 B. Bergman, E. Fontes, C. Lagergren, G. Lindbergh, A. Lundblad, S. Schwartz, D. Simonsson and C. Sylwan, *Proc. 1992 Fuel Cell Seminar, Tucson, AZ, USA, Nov. 29–Dec. 2, 1992,* p. 73.
19 H. Koch, B. Rohland and H. Wendt, *Proc. 1992 Fuel Cell Seminar, Tucson, AZ, USA, Nov. 29–Dec. 2, 1992,* p. 277.
20 S.H. Lu and J.R. Selman, *J. Electrochem. Soc., 131* (1984) 2827.
21 A. Pozio, *Thesis,* University of Rome, Dec. 1991.
22 M. Stefanoni, unpublished work.
23 B.A. Boukamp, *Solid State Ionics, 20* (1986) 31.
24 *Handbook of Chemistry and Physics,* The Chemical Rubber Co., Cleveland, OH, 46th edn., 1964.
25 G. Liptay, *Atlas of Thermoanalytical Curves,* Heyden and Son, London.
26 R.J. Gummow, D.C. Liles and M.M. Thackeray, *Mater. Res. Bull., 28* (1993) 235.
27 J.B.J. Veldhuis, F.C. Eckes and L. Plomp, *J. Electrochem. Soc., 139* (1992) L6–L8.
28 L.J. Van der Pauw, *Philips Res. Rep., 13* (1958) 1–9.
29 J. Molenda, A. Stoklosa and T. Bak, *Solid State Ionics, 36* (1989) 53–58.
30 A. Bielanski and J. Deren, *Proc. Symp. Electronic Phenomena in Chemistry and Catalysis on Semiconductors,* De Gruyter, Berlin, 1969, p. 149.
31 L. Giorgi, E. Simonetti and A. Pozio, *Proc. 1992 Fuel Cell Seminar, Tucson, AZ, USA, Nov. 29–Dec. 2, 1992,* p. 554.
32 P. Tomczyk, G. Mordarski and J. Oblakowski, *J. Electroanal. Chem., 353* (1993) 177–193.
33 R.E. Meredith and C.W. Tobias, *Advances in Electrochemistry and Electrochemical Engineering,* Vol. 1, Interscience, New York, 1960, pp. 15–47.
34 D.A.G. Bruggeman, *Ann. Phys., 24* (1935) 636.
35 L. Giorgi, E. Simonetti and A. Pozio, *Proc. 2nd Int. Symp. Electrochemical Impedance Spectroscopy, Santa Barbara, CA, USA, July 11–17, 1992.*
36 L. Giorgi and M. Carewska, in preparation.
37 I. Uchida, T. Nishina, G. Lindbergh and T. Kudo, *Proc. Int. Fuel Cell Conf., Makuhari, Japan, July 3–6, 1992,* p. 189.
38 A.J. Appleby and S.B. Nicholson, *J. Electroanal. Chem., 112* (1980) 71.
39 A.J. Appleby and S.B. Nicholson, *J. Electroanal. Chem., 83* (1977) 309.
40 A.J. Appleby and S.B. Nicholson, *J. Electroanal. chem., 53* (1974) 105.
41 I. Uchida, T. Nishina, Y. Mugikura and K. Itaya, *J. Electroanal. Chem., 206* (1986) 229.